Translocation of a globular polymer through a hairy pore

Alexander Mair,[1] Clarion Tung,[2] Angelo Cacciuto*,[2] and Ivan Coluzza[3,*]

[1]*Faculty of Physics, University of Vienna,*
Boltzmanngasse 5, 1090 Vienna, Austria
[2]*Department of Chemistry, Columbia University,*
3000 Broadway, New York, NY 11201
[3]*CIC biomaGUNE, Parque Cientfico y Tecnolgico de Gipuzkoa,*
Paseo Miramn 182, 20014 Donostia/San Sebastin, Gipuzkoa. Spain.

Abstract

We present numerical simulations of a globular polymer translocating through a cylindrical pore internally coated with a polymer brush. We first characterize the statistical properties of the brush under flow and show how, at high grafting densities, the monomer profile of the brush is unaffected by the presence of the fluid flow. We then exploit the fluid flow to force a globular polymer through it and study how it deforms as a result of the interaction with the brush. Finally, we discuss how such a setup could be used as a protein purification device.

PACS numbers: 87.15.Cc, 05.20.-y, 87.10.Rt

Introduction

The three-dimensional conformation acquired by a protein in its functional form (native structure) is controlled by the sequence of amino acids along the protein backbone. The native structure is often unique for a given sequence. However, many catastrophic events can take place when just a few proteins fail to reach their functional configuration [1]. A significant obstacle along the correct folding pathway occurs when a protein aggregates with other copies of itself. The formation of large protein clusters can be lethal to cells and, in the long run, can lead to neurodegenerative diseases such as Alzheimer and Parkinson disease [2–5]. Furthermore, protein aggregates present a significant obstacle in protein purification technology [6, 7]. Since unregulated protein aggregation poses an important threat to life in all living organism, under evolutionary pressure, complex protection mechanisms against it have been set in place [8–11].

In prokaryotic cells, for instance, the GroEL/GroES chaperonin complex acts as an efficient protection against misfolding and aggregation. The GroEL/GroES chaperonin is a double-barrelled complex with two large cavities where misfolded proteins are captured and isolated for a long time ($\sim$ 15s) and at considerable energy cost (7 ATPs per protein or 14 ATPs per cycle). The working principle of the GroEL/GroES has not been fully elucidated, but its primary function is to segregate misfolded proteins from the cytosol into a molecular cage to prevent their unregulated aggregation with other proteins. Furthermore, the GroEL is believed to help misfolded proteins captured in its interior to refold into their native state. Recently, a new refolding reaction pathway for the GroEL/GroES complex has been postulated [12, 13]. Coluzza et al. hypothesised that confinement inside the cage could induce protein translocation through the equatorial region that connects the two chambers, and suggested that the translocation process could help proteins escape local free energy minima regardless of their specific amino acid sequence. Although such a pathway has not been experimentally investigated, it offers an appealing design principle for the development of an artificial device that could be used to promote the correct folding path of a protein and bypass their detrimental aggregation. Inspired by this idea, in this work we consider the translocation of a globular polymer, that we will use a crude model for a misfolded globular protein, through a cylindrical pore whose inner surface is coated with a soft polymer brush. We explore the complex interactions between the polymer, the brush, and the solvent, to understand under what conditions such a system could be useful as a device to refold misfolded proteins and/or break up the aggregates they form. The idea is to push the globular

polymer through the pore using a flow field in the solvent and exploit the shear forces that develop from the interaction of the protein with the soft brush to break up agglomerates and unfold misfolded states. Crucially, a moving fluid in a pipe would itself generate shear forces due to the parabolic (Poiseuille) profile of the velocity field, even in the absence of the brush, and it has been shown in experiments and computer simulations, that large protein multimers like the von Willebrandt factor (vWF) can unfold[14–16] as a result of the shear forces applied on the protein by a moving fluid. A recent review addresses the topic of shear-induced protein unfolding by comparing multiple experimental and theoretical studies on different proteins [17]. In most of these experimental setups, special flow devices are used to exert shear on the proteins in solution. Many of these experimental studies find an effect on the proteins function (or activity for enzymes) at moderate shear rates of 10^2 - 10^5 s^{-1}. However, the experiments in some of these devices include an air-water interface which can also contribute to a loss of protein functionality. In a different paper, *Jaspe et al.* [18] investigated the behavior of a small protein in a channel of diameter equal to 180 μm. The fluid was pushed through the channel by a pressure drop leading to shear rates up to 10^4 s^{-1}. The authors found no sign of a significant structural change in the protein structure, and proposed a simple theoretical model to estimate the onset shear rate required to unfold their proteins. This is expected to be of the order of 10^7 s^{-1}, which is very hard to achieve in small channels [19]. The question of whether small proteins can unfold in physical shear flow remains controversial, whereas the induction of structural changes driven by fluid shear in larger complexes such as vWF is widely accepted [17].

Here, we present an explicit study of the unfolding pathway of a globular polymer driven by a fluid flow through a cylindrical pore coated with a deformable polymer brush. The goal is to understand under what conditions the presence of the brush can improve the refolding rate of the globular protein. Such an approach, combined with the scaling properties of the brush, offers the advantage that the setup can be scaled up to large pores that allow for fast flow velocities and a smaller likelihood of pore clogging by protein aggregates.

Although the equilibrium interactions between free chains with a cylindrical brush have been extensively characterized [20], to the best of our knowledge, there has been no study investigating the ability of a brush to deform a globular polymer under flow. Of relevance to our work is also the study by *Mahmood et al.* [21] who discussed the potential of a DNA-grafted cylindrical pore to function as a biosensor under the influence of an electrical field. Furthermore, studies on unfolding of polymer globules [22], translocation under flow of star-

polymers in a slit channel [23] and rod-like proteins in both slit and cylindrical geometries [24] have also been recently published.

Methods

Throughout this paper, we will represent our data in dimensionless Lennard-Jones units, for which the fundamental quantities mass m_0, length σ_0, epsilon ϵ_0, and the Boltzmann constant k_B are set to 1, and all of the specified masses, distances, and energies are multiples of these fundamental values corresponding to $T = T_0 = \epsilon_0/k_{\mathrm{B}}$, $m = m_0$, $\sigma = \sigma_0$, and $\tau_0 = \sqrt{\frac{m_0\sigma_0^2}{\epsilon_0}}$.

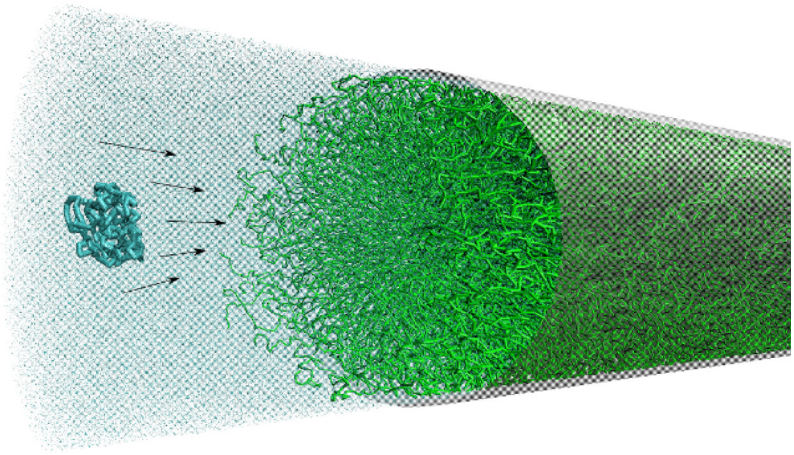

FIG. 1: Visualization of the relevant components of our system. The blue folded chain represents the protein model while the green chains are the polymers grafted to the cylinder walls forming the brush. The arrows indicated the direction of the fluid flow pushing the protein through the brush. The light blue dots indicate the SRD fluid particles.

Each polymer grafted on the inner surface of the pore of radius R is described as a sequence of spherical beads of diameter σ. Excluded volume interactions between any two monomers are enforced via a Weeks-Chandler-Anderson (WCA) potential

$$U_{\mathrm{WCA}} = 4\epsilon\left[\left(\frac{\sigma}{r}\right)^{12} - \left(\frac{\sigma}{r}\right)^{6} + \frac{1}{4}\right] \tag{1}$$

extending up to $r_c = 2^{\frac{1}{6}}\sigma$ with $\varepsilon = k_BT$. Connected monomers along the chain are held

together with a FENE potential of the form

$$U_{\mathrm{FENE}} = \frac{KR_0^2}{2} \ln \left[1 - \left(\frac{r}{R_0} \right)^2 \right] \tag{2}$$

Where $R_0 = 1.5\sigma$ is the maximum bond length and $K = 30k_BT/\sigma^2$ is the strength of the bond. The surface of the cylinder is covered with densely packed WCA spherical particles of diameter σ arranged according to an hexagonal lattice with lattice constant equal to σ. These particles are locked in place during the simulation, and each polymer has its first monomer linked to one of them with the same FENE potential described above. The pore extends along the x axis of our simulation box up to a length L_p and contanins N_p polymers of length N_m, at a grafting density $\rho_G = N_p/(\pi R^2 L_p)$.

The polymer that translocates through this pore is described in a similar manner, with the exception that each of its 200 monomers of diameter σ is connected to its neighbor with harmonic bonds with a minimum at σ and spring constant $\kappa_0 = 200k_{\mathrm{B}}T$. The strong spring constant is equivalent to a constant bond length equal to σ as in the protein models by Honeycutt and Thirumalai [25]. The monomers interact with a Lennard-Jones potential of the form:

$$U_{\mathrm{LJ}} = 4\epsilon \left[\left(\frac{\sigma}{r} \right)^{12} - \left(\frac{\sigma}{r} \right)^{6} \right] \tag{3}$$

The cutoff is set to 2.5σ and $\epsilon = k_{\mathrm{B}}T$, which yields a globular polymer at equilibrium. The solvent is described by multiparticle collision dynamics, also known as stochastic rotation dynamics (SRD), a particle-based mesoscopic method used to reproduce hydrodynamic flow fields and solute interactions. The method consists of two steps. In the streaming step, particles move according to $\mathbf{r_i}(t+\Delta t_{SRD}) = \mathbf{r_i}+\mathbf{v_i}\Delta t_{SRD}$. In the collision step, SRD particles are assigned to cubic bins of length Δx, the center of mass velocity $\mathbf{v_{cm}}$ is calculated, and the relative velocities are rotated by an angle α about a random axis, according to $\mathbf{v_i}(t + \Delta t_{SRD}) = \mathbf{v_{cm,i}}(t) + \Omega(\alpha)(\mathbf{v_i}(t) - \mathbf{v_{cm,i}}(t))$, where Ω is a rotation angle. We set the SRD particle mass $m_{SRD} = 0.1m$, the average particles per bin $\rho = 10$, the bin size $\Delta x = \sigma$, the SRD timestep $\Delta t_{SRD} = 0.01\tau$ and rotation angle $\alpha = 120°$, giving a fluid viscosity of $\eta = 7.55$. All monomer masses are set to $m_M = \rho m_{SRD}$ and are coupled to SRD particles in the collision step. Solvent flow is induced by applying a constant acceleration a to all solvent particles, and all subsequent values are reported in units of σ/τ^2. SRD particles are confined within hard cylindrical walls with the same axis and radius R as the pore, and length L spanning the length of the simulation box with periodic boundary conditions. To accurately represent no-slip boundary conditions at the walls of the cylinder, we use the

bounce-back and bulk-filling rules described by Lamura [26].

Figure 1 shows a typical snapshot of the system including all components considered in this study, i.e. the cylindrical channel, the pore, the brush and the globular polymer.

Finally, the repulsion between any monomer and the walls of the cylinder is described using a WCA potential of the form

$$U_{\text{Wall}} = 4\epsilon \left[\left(\frac{\sigma}{(R_i(y,z) - R)} \right)^{12} - \left(\frac{\sigma}{(R_i(y,z) - R)} \right)^{6} + \frac{1}{4} \right] , \tag{4}$$

with $\epsilon = k_{\text{B}}T$ and cutoff $2^{\frac{1}{6}}\sigma$. Here $(R_i(y,z) - R)$ is the radial distance of monomer i from the surface of the cylinder, and R is the cylinder radius. In this work we considered two pore sizes, one of radius $R = 9.55\sigma$ and the other $R = 19.1\sigma$. Before the globular polymer is translocated through the pore, the brush is equilibrated in the presence of the fluid flow.

Our simulations are performed using a timestep of $\Delta t = 0.002\tau$ and simulations are run for a minimum of 10^8 timesteps.

Given the large number of parameters associated with this system, and the lengthy nature of the simulations with an effective, yet explicit fluid, we are limited to study a subset of possible parameters. We considered three explicitly brush setups separately. The first case, **Case 1**, is characterized by a pore of radius $R = 9.55\sigma$, length $L_p = 71.7\sigma$, and grafting density $\rho_G = 0.28$. In this case we considered brush polymer chains with $N_m = 10, 11, 12, 14$ monomers, as larger values of N_m would overfill the pore. The second case, **Case 2**, is characterized by a pore with the same radius and length as in case 1, but with a smaller grafting density $\rho_G = 0.07$. Here, we considered brush polymers consisting of $N_m = 20, 30, 40$ and 50 monomers. Finally, the third case, **Case 3**, is characterized by a pore of $R = 19.1\sigma$, $L_p = 103.1\sigma$ and $\rho_G = 0.28$, a setup essentially equivalent to case 1 with a pore diameter twice as large. For this case, we considered brush polymers with $N_m = 20, 22, 24$ and 26 monomers. To study the crucial finite size effects introduced by the boundaries of the pore we considered simulation boxes of lengths $L > L_p$. For case 1 we selected $L = 92.7\sigma$, for case 2 we selected $L = 112.7\sigma$, and for case 3, we set $L = 183.1\sigma$. For all cases, we considered fluid accelerations in the range $a \in [0.0, 0.1]$, corresponding to Reynold's numbers ranging from $Re \in [0.0, 0.05]$. As a reference, if we consider a large multimeric protein like the vWF-factor, and set $\sigma = 80nm$, that would give a pressure drop $\frac{\Delta p}{\Delta L} = 0.9$ bar/mm for $a = 0.1$.

RESULTS AND DISCUSSION

This section is divided in two parts. In the first part we characterize the behavior of the pore for different values of the fluid velocity, brush density, brush height and overall pore diameter. In the second part we consider the actual translocation events of a globular polymer through the pore.

Characterization of the pore

We start our analysis by characterizing the behavior of the brush under the influence of the fluid flow and in the absence of the globular polymer. This is important because, intuitively, one would expect that when the brush is long enough to fill the pore, a translocation event will force a globular polymer to deform as it squeezes through it. In the opposite case, when the brush profile allows for a monomer-free region at the center of the pore much larger than the radius of gyration of the globular polymer, the globule can translocate through the pore with minimal disturbance from the brush. An optimal brush will have a monomer density gap along the pore axis whose size is comparable or smaller than the size of the protein.

Let's first consider **Case 1**. Figure 2 shows a typical steady state configuration of the brush under a flow with $a = 0.1$. The side-view and the cross-section are shown independently, and a small monomer density gap can be observed at the pore center.

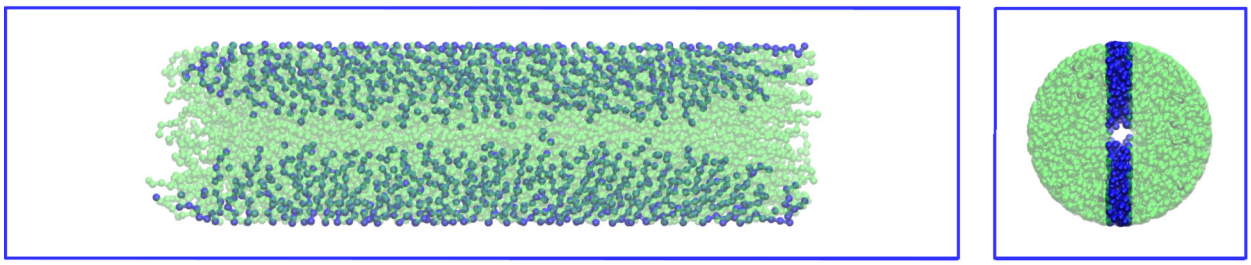

FIG. 2: Snapshot of a cylindrical brush under flow for **Case 1** (see text for pore parameters) , showing the side view on the left panel and the cross section on the right panel. Several chains are depicted in blue to show individual chain conformations. The solvent particles are not shown. The brush has chain length of $N_m = 10$ and the fluid acceleration is $a = 0.1$ and $R = 9.55\sigma$

.

Figure 3 shows both the radial profile of the axial velocity of the fluid and the monomer density profile for $a = 0$ and $a = 0.1$. The density profile under flow is almost identical

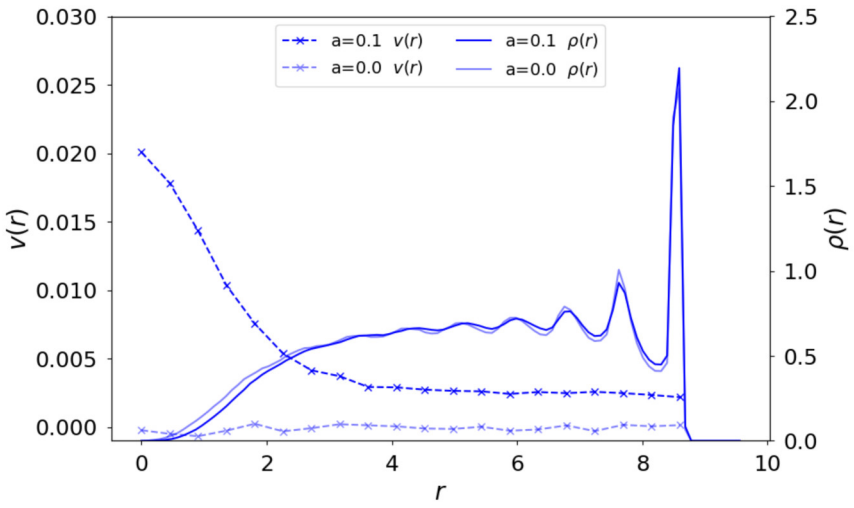

FIG. 3: Brush monomer density and solvent flow profile for $a = 0$ and $a = 0.1$ for the setup in case 1 and $N_m = 10$.

to the one at equilibrium, and it is characterized by a density gap at the pore center and increasing monomer density approaching the wall. Significant layering effects are seen near the wall due to the high grafting density. The solvent flow profile for $a = 0.1$ shows a non-insignificant fluid velocity along the axis of the pore, followed by a long plateau that persists deep into the brush until it finally drops to zero at the cylinder wall. To properly handle the no-slip boundary condition at the cylinder wall, we modified the default SRD implementation in LAMMPS [27] to include the corrections discussed in *Lamura et al.*[26]. Simulations of the fluid flow inside the cylinder when no polymer brush is included show an insignificant slip of the fluid near the wall. It is not clear to what extent the long and weak plateau observed for $r > 4$ is an artifact of the specific coupling of the SRD particles and the monomers, or this can be understood, even at such a small length-scales, through the frame of Darcy's law describing a fluid flow in a porous medium. Either way, this effect is rather weak and should have no significant impact on our results on the translocation of the globular polymer through the pore.

We now investigate how increasing chain length N_m changes the monomer density and solvent velocity profiles at $a = 0.1$, and Figure 4 shows the results of this analysis.

The main change in the density and velocity profiles occurs at the center of the pore. As N_m increases, the monomers gradually and systematically fill the density gap at the pore center. As expected, the decrease of the size of the density gap at the pore center is followed by a significant drop in the flow velocity profile. These data indicate that when the brush

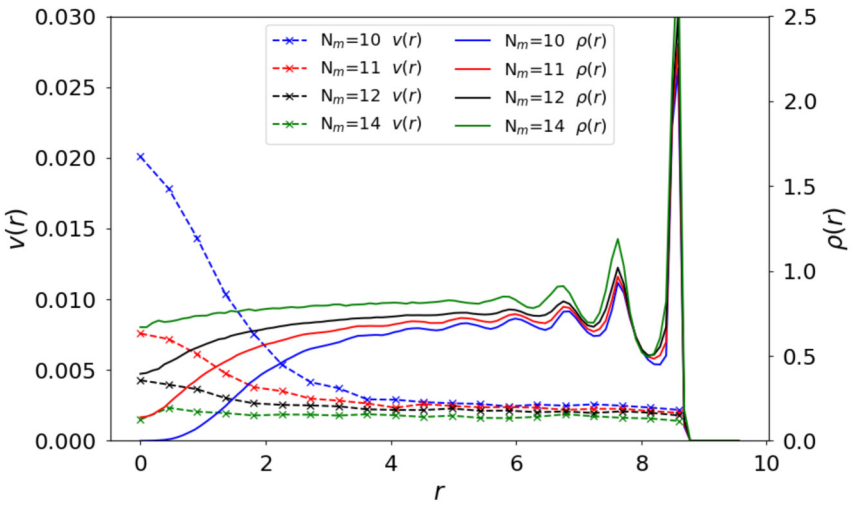

FIG. 4: Monomer density and solvent flow profiles for different chain lengths N_m for the setup in case 1 with $a = 0.1$. As the chain length N_m increases, the monomers fill the center of the core and the solvent velocity decreases.

polymer chains are too long the pore becomes effectively clogged against the solvent flow, thus making for a poor candidate as a device for refolding translocating globular polymers. In the opposite limit, when the brush is too short, no significant interactions between the brush and a translocating globule can be established due to a density gap that would be larger than the radius of gyration of the globule. We identify $N_m \approx 10$ as an optimal candidate under these solvent flow conditions, as there is still a sizable density gap at the pore center that allows for solvent flow.

Snapshots of the brushes show that along the pore's cylindrical axis, the monomer density is mostly uniform in the middle but varies greatly at the edges of the pore, due to the splay of the individual polymers exiting the pore. A detailed analysis of the orientation ϕ of the brush with respect to the flow velocity is presented in the Appendix. In summary, the brush acquires a symmetric shape at the center of the pore ($x = L_p/2$) at equilibrium ($a = 0$), with $\phi \simeq 90$ in the middle, $\phi > 90$ for $x < L_p/2$, and $\phi < 90$ for $x > L_p/2$. As the flow acceleration a increases, the average value of ϕ across the pore becomes smaller, indicating that the brush begins to tilt towards the direction of the flow. Interestingly, the polymers at the pore entrance ($x \simeq 0$) point against the flow $\phi > 90$ even for large flow values of a (the larger N_m the stronger this effect), while at the pore exit ($x \simeq L_p$) the polymers are well stretched in the direction of the flow ($\phi \simeq 20$ degrees). We also find the degree of tilting to be rather insensitive to different chain lengths N_m near the middle of the brush, and that

the density profile of the brush computed by only considering polymers the middle of the brush is independent of the fluid acceleration a (data not shown). This suggests that at this grafting density the tilting polymers must compensate for the unchanged brush height by stretching.

Let's now consider the second pore considered in this study: **Case 2** with lower grafting density. The lower grafting density makes the brush more deformable under solvent flow. Here, the brush acquires large tilt angles for large flows and it compresses against the wall. The monomer density profiles both with and without solvent flow are shown in Fig. 5. At $a = 0$, monomers fill the pore center, but at $a = 0.1$, a large density gap develops in the center of the pore and the monomer density near the walls increases as a result of the brush compression against the walls of the cylinder. The solvent velocity profile shows a parabolic functional form at the pore center. Fig. 6, shows how the density and velocity profiles change

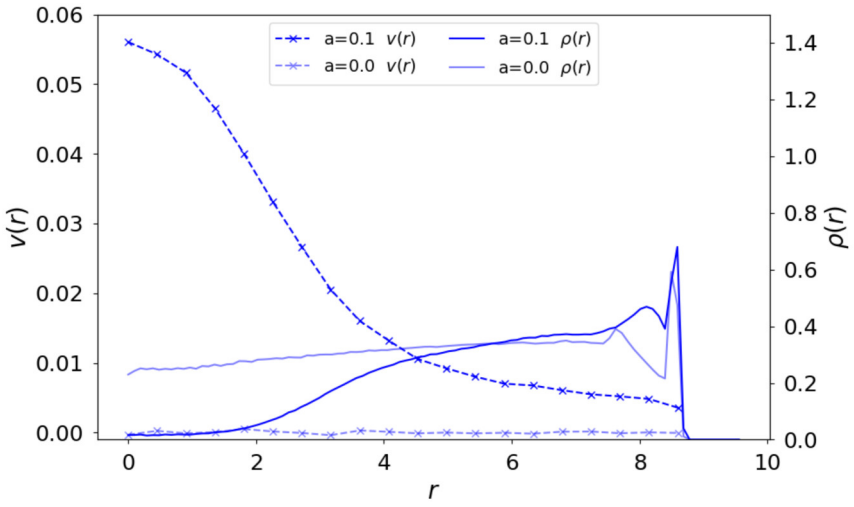

FIG. 5: Brush monomer density and solvent flow profile for $a = 0$ and $a = 0.1$ for the setup in case 2 and $N_m = 20$.

upon increasing the length of the polymers N_m.

Crucially, when comparing **Case 1** with $N_m = 10$ and **Case 2** with $N_m = 40$, two brushes with the same overall monomers density inside the cylinder, we find that in the system with the lower grafting density (**Case 2**) the pore is completely occluded by the monomers, whereas the pore with the higher grafting density (case 1) shows a sizable monomer density gap at its core. This indicates that the grafting density plays a crucial role on the overall conformation of the brush under flow. To better characterize the brush conformation in the presence of the fluid flow, we also measure the brush tilt angle ϕ as before. A study of

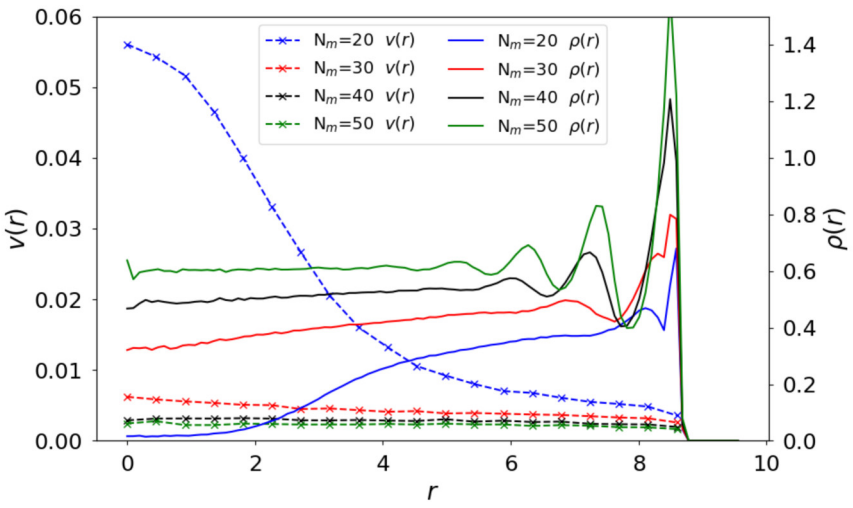

FIG. 6: Monomer density and solvent flow profiles for different chain lengths N_m for the setup in case 2 with $a = 0.1$. As the chain length N_m increases, the monomers fill the center of the core and the solvent velocity decreases.

the brush tilt angle as a function of the flow for different polymer lengths shows that (see appendix for details) at this low grafting density, the brush tilts much more sharply than in **Case 1**, and already for $a \geq 0.05$, the brush is already fully stretched throughout the length of the pore. Furthermore, as was the case for the pore with higher grafting density, the tilt angle, in the middle of the pore, ($x \simeq L_p/2$), seems to be rather insensitive to the chain length N_m.

Given the strong dependence of the density profile on the fluid flow for **Case 2**, it is more difficult to control the size of the monomer density gap, which is a critical design parameter for a refolding device. Furthermore, the configuration of the brush at the target acceleration $a = 0.1$ consists of stretched polymers aligned along the direction of the flow throughout the pore, forming what is basically a soft funnel that is unlikely to generate sufficiently large shear forces on a translocating globular polymer.

We now turn our attention to **Case 3** which is a pore with twice the radius but the same grafting density as the pore in **Case 1**. We emphasize that we keep the same maximum applied fluid accelerations $a = 0.1$ used in the other two cases. This clearly results in a larger fluid velocity inside the pore as expected from Poiseuille's law. We made this choice because we want to investigate how a change of the channel radius would affect velocity and density profiles inside the pore while keeping the fluid driving force constant. Because of the faster fluid inside the pore, overall, we expect the brush shows a more substantial

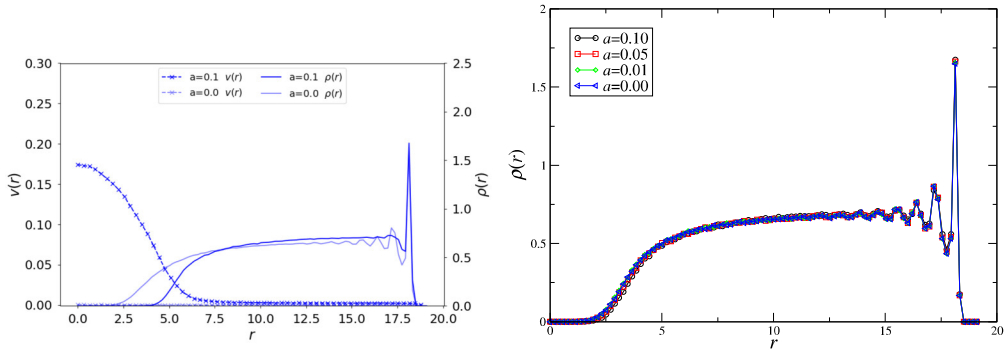

FIG. 7: Brush monomer density and solvent flow profile for $a = 0$ and $a = 0.1$ for the setup in case 3 and $N_m = 20$. The left panel shows the result when averaging over the who extent of the pore, while the right panel shows the same data when only considering the polymer in a 10σ shell the middle of the pore, i.e. for $x = L_p/2$.

tilt than in **Case 1**, but not as dramatic as it is in the brush at lower grafting density in **Case 2**. Figure 7(left) compares monomer density and solvent velocity profiles for the driven ($a > 0$) and the equilibrium systems ($a = 0$). In the presence of a fluid flow, the monomer density near the walls is similar to that at equilibrium, albeit with weaker layering, and the size of the monomer density gap at the center of the pore is somewhat wider than that at equilibrium. This result would suggest that unlike the behavior of the pore in **Case 1**, not only the chain conformation, but also the size of the monomer density gap depend on a. A more careful analysis that only considers the monomer density profile around the middle of the pore ($x \simeq L_p/2$), which should minimize the effect of the larger edges at the pore opening and exit, reveals that this is not the case, and as observed in **Case 1** with the smaller pore radius, the monomer density distribution $\rho(r)$ is independent of a. The result of this analysis is shown in Fig. 7(right). The effect on the density profile due to increasing the chain length N_m is shown in Fig. 8. The data indicate a systematic filling of density gap followed by a decrease of the flow velocity within it as N_m increases. A detailed study of the tilt angle of the brush along the pore for different values of a is presented in the appendix. Here, we summarize the results by mentioning that, as in **Case 1**, the front of the pore is characterized by a layer of polymers that resist pointing in the direction of the flow even at the highest driving forces (this effect becomes more evident as one increases N_m) while the back side of the brush adapts to the flow. We also observe, as was the case in the previous two cases, that while ϕ decreases with fluid acceleration, it remains basically independent of the number of monomers in the polymer brush, N_m, for a fixes value of a.

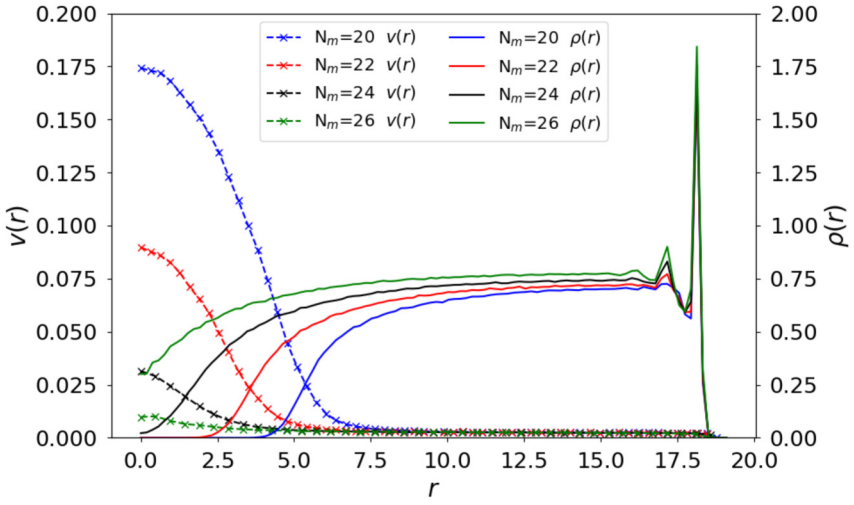

FIG. 8: Monomer density and solvent flow profiles for different chain lengths N_m for the setup in case 3 with $a = 0.1$. As the chain length N_m increases, the monomers fill the center of the core and the solvent velocity decreases.

It is important to stress that since the statistical properties of the pores coated with the polymer brushes at the highest grafting densities are independent of the presence of the fluid flow, at least when it comes to the density profile and the size of the monomer-free gap along the pore axis, it should be possible to systematically scale up the pore diameter, as we did going from **Case 1** to **Case 3**, and use standard equilibrium arguments to estimate the expected brush height in the pore [28] even when in the presence of the fluid flow. This is important because larger pores have the advantage of generating larger flow velocities in their cores at a fixed driving force, are less likely to be clogged by protein aggregates, and are easier to fabricate. Furthermore, as discussed by Dimitrov et al. [29] (and references therein), a convenient property of cylindrical polymer brushes is that as the tube diameter increases, the reduced brush height h/N_m decreases. This allows for a finer control of the brush height with the chain length N_m, and thus a better control of the monomer density gap at the pore center.

Before we start discussing the results relative to the actual translocation events, it is worth noting that several studies on polymer brushes under shear have been published, and, consistently with our results (at least in the large grafting density regime), the brush height is expected to be rather insensitive to the applied shear rate [30–32]. It should be stressed, however, that most of these works were performed on planar brushes of infinite extension. In our system, we considered finite-sized pores, and in our data, as discussed above, edge effects

can become important when studying the statistical properties of the brush. Although we expect the data collected in the middle of the brush at $x \simeq L_p/2$ to be rather insensitive to the boundaries, for a systematic study of the scaling laws of a cylindrical polymer brush under shear, one should ideally consider a setup where the side length of the simulation box equals the length of the pore ($L = L_p$) with periodic boundary conditions to mimic the behavior of an infinitely long pore. This is not that study, because as it turns out, the effect of the edges is crucial when considering the translocation of the globular polymer through the pore. In fact, the largest shear forces develop at the pore exit as the globular polymer moves from a high monomer density region to a depleted one.

Translocation events

We identify the brush with $N_m \simeq 10$ in **Case 1** and the brush with $N_m \simeq 24$ in **Case 3** as the most promising re-folders. In both cases the brush grafting density is sufficiently large that the monomer density profiles in the middle of the pore are not affected by the solvent flow, and a sufficiently wide monomer density gap is available to interact with the globular polymer without dramatically reducing the velocity of the flow through the pore. As the globular polymer translocates through the pore, we characterize its degree of distortion using its radius of gyration R_g. As a reference the radius of gyration of our globular polymer with 200 monomers at equilibrium is measured to be $R_g = 3.09\sigma$. The polymer theta point was measure to be at roughly $T_\theta = 2$ [33].

Figure 9 shows the three main stages, entrance (top panel), traveling (middle panel), and exit (bottom panel) of the typical translocation process in the pore of radius $R = 9.55\sigma$. The initial deformation of the globular polymer occurs as it enters the pore and is pushed through the monomer density gap against the brush; here the brush polymers are on average pointing against the direction of the flow. As the globular polymer moves through the pore, it is elongated along the cylindrical axis by the radial pressure exerted by the surrounding brush. The conformation of the brush polymers at the end of the pore are on average pointing along the direction of the flow. As the globular polymer exits the pore, it crosses a significant monomer density gradient. While exiting, one part of the globular polymer is in a monomer-free region while the other still feels the radial pressure of the brush. This monomer gradient creates an effective elongational shear at the end of the pore that further destabilizes the conformation of the globular polymer. Once outside the pore, the polymer

re-folds into a globular state in a monomer-free environment. Fig. 10 shows the radius of

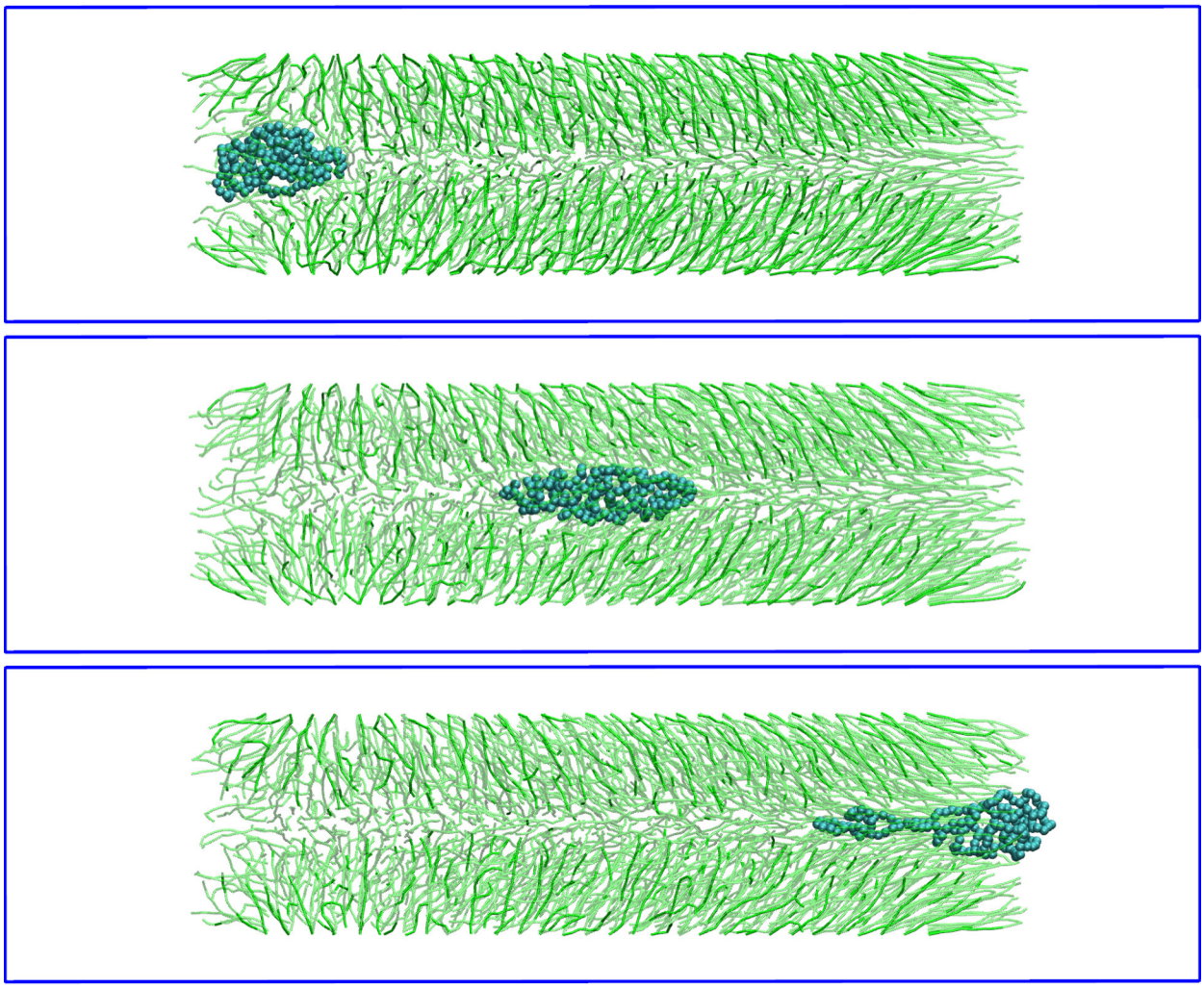

FIG. 9: Three snapshots from our simulations showing the translocation process of a globular polymer for the **Case 1** pore, for $a = 0.1$ and $N_m = 11$. From top to bottom: the globular polymer pore entering the pore, the polymer in the middle of the pore, and the polymer exiting the pore. At the exit, additional shear forces arise due to the significant monomer density gradient.

gyration R_g as a function of time as the globular polymer translocates through the pore, for multiple translocation events. Here the effect of the pore exit is clearly marked by a sharp peak in R_g at the end of each translocation event. Also notice how when increasing the length of the brush, the translocation time increases (top/middle panel), until, when $N_m = 12$ the velocity profile inside the pore becomes too weak to drive the globule through it. The figures in the bottom panels show the position of the protein along the axial direction of the pore as a function of time for the different values of N_m. Here the x coordinate is propagated and includes the crossing of the periodic boundaries so that the globular protein

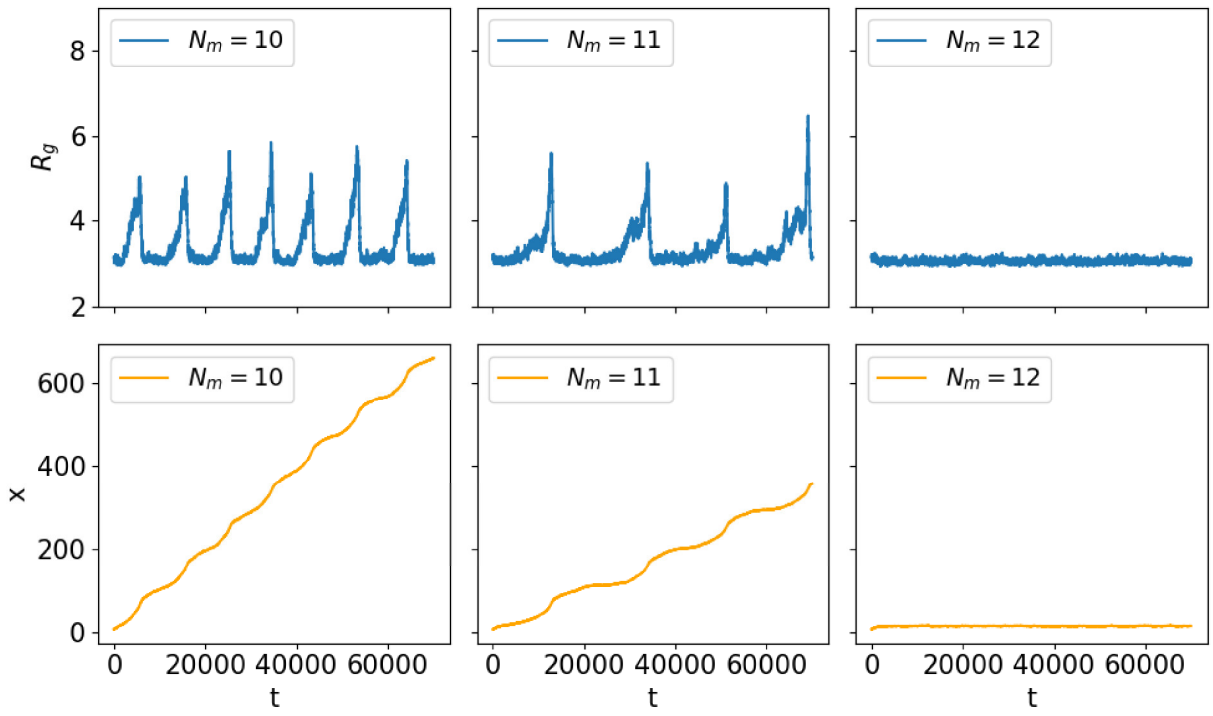

FIG. 10: The top row shows the radius of gyration R_g of a globular polymer undergoing repeated translocation through the **Case 1** pore, with flow $a = 0.1$. The chain length N_m increases from left to right. The bottom row shows the corresponding position of the polymer, and at chain length $N_m = 12$, the polymer cannot enter and the pore is essentially clogged.

goes through a series of translocation events over time within the same simulation.

Figure 11 shows snapshots of the translocation process for the larger **Case 3** pore with $N_m = 24$. We again see two stages of deformation, at the entrance and at the exit of the pore, and the exiting process is even more dramatic than in the smaller **Case 1** pore. The flow velocity for $N_m = 24$ in the middle of the pore is more than twice as that for $N_m = 11$ in the **Case 1** pore with the smaller diameter, suggesting that scaling up the channel has the advantage of being able to translocate larger globules more quickly and generate larger shear forces. Crucially, the larger pore allows for a wider range of brush heights, and corresponding monomer density gaps, to successfully refold the globules. This suggests that larger pores should make more robust re-folders. This is most evident in Figure 12 (top/right panel) that shows larger R_g excursions than those observed for the smaller radius. As expected, the trajectory for $N_m = 20$ (Top/Left) shows more frequent deformation peaks than those at higher monomer concentration as the velocity inside the pore decreases with N_m. While, on the one hand, having a lower monomer density allows for more refolding event, on the other

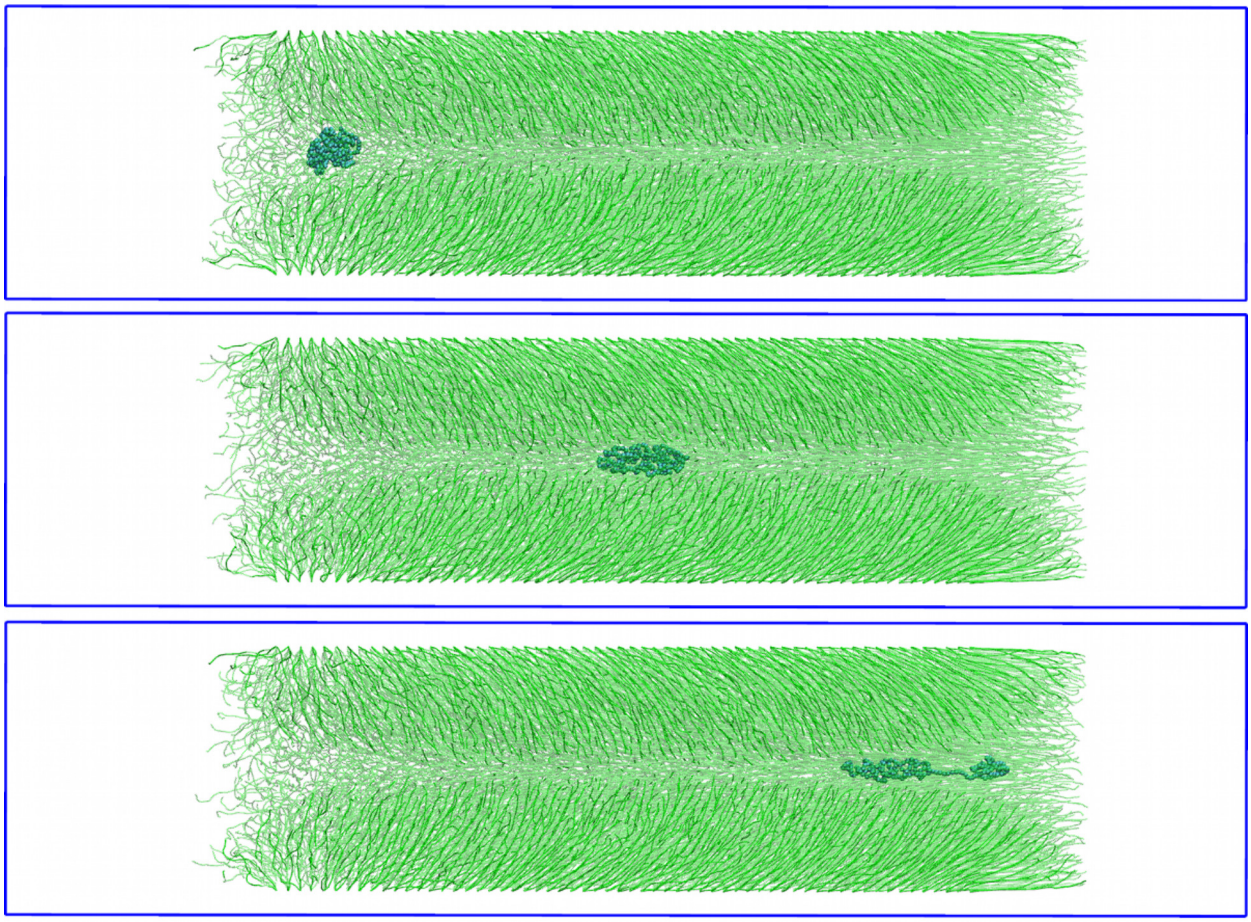

FIG. 11: Three snapshots from our simulations showing translocation of a globular polymer through the larger **Case 3** pore with $a = 0.1$ and chain length $N_m = 24$. From top to bottom: the polymer enters the pore, the polymer in the middle of the pore, and the polymer just before exiting the pore.

hand the extent of the deformation become larger, although less frequent, when increasing the monomer density. Ideally, one would like to setup a system that optimizes these two tendencies.

Conclusion and outlook

In this paper we considered whether a globular protein, modeled as a globular homopolymer, could be forced to undergo conformational changes when translocating through a cylindrical nanopore internally coated with a polymer brush. We studied the brush profile in the presence of a fluid flow for different values of monomer concentrations, grafting density, and for two pore sizes. Crucially, we find that the influence of the flow on the brush conformation

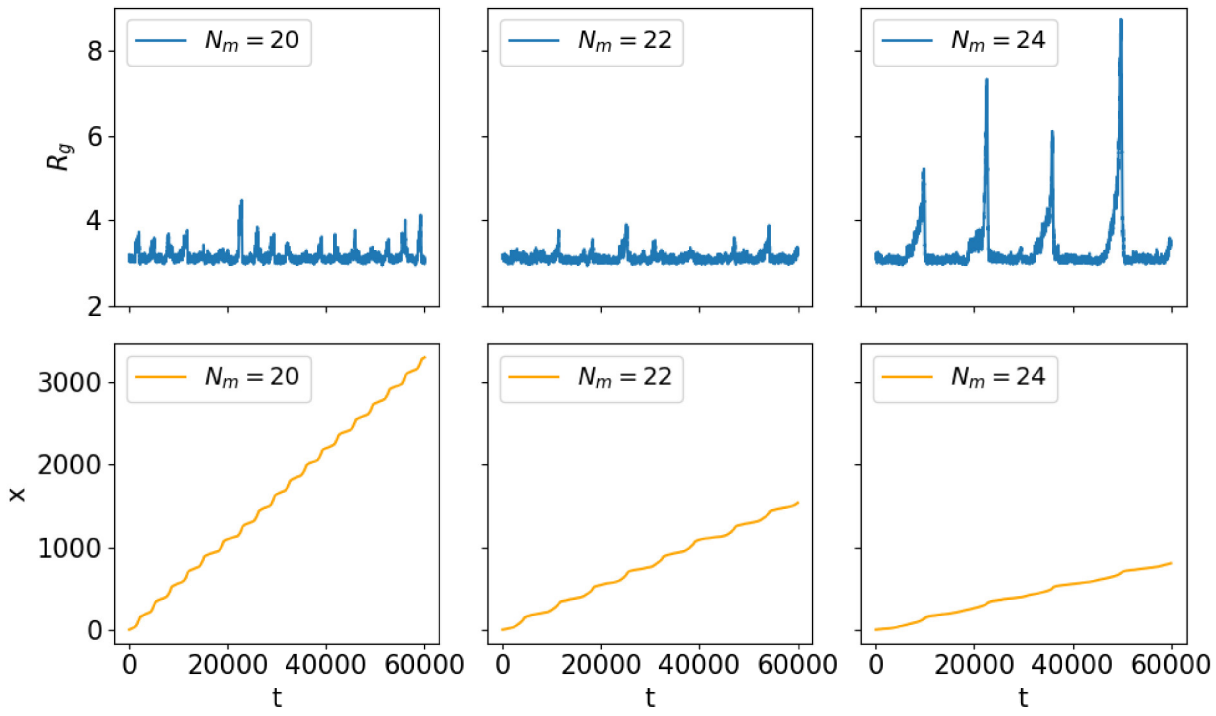

FIG. 12: The top row shows the radius of gyration R_g of a globular polymer undergoing repeated translocation through the **Case 3** pore, with flow $a = 0.1$. The chain length N_m increases from left to right. The bottom row shows the corresponding position of the polymer. The larger pore allows for finer control of the monomer density gap via N_m, which in turn allows for better control of the polymer distortion during translocation.

strongly depends on the grafting density of the brush, and when ρ_G is sufficiently large, the density profile of the brush is not affected by the presence of the flow, yet the fluid velocity within the pore is very much dependent on the overall monomer concentration (brush height), and drops to small values once the pore becomes completely filled with monomers.

We observe that under the appropriate conditions, high grafting density and sufficiently long chains to leave a small monomer gap along the pore axis, the interaction of the globule with the brush can indeed cause significant deformations of the globule. The globule entrance into and exit from the pore events are of particular interest as they lead to the largest distortions of the globules conformation.

While in this study our protein model, described as a globular polymer, is very rudimentary, tests with a more realistic protein model, retaining some of the specificity of the monomer-monomer interactions that is proper to proteins, are underway and look promising. We believe that the ease with which our protein models deforms within the pore is due,

in part, also to the large number of intermediate states that can be accessed by the globular homopolymer without a significant loss of interaction energy. For a protein with more specific interactions, the number of low energy misfolded configurations should be much smaller, and the translocation should lead to more significant structural changes throughout the process. Given the large effect the edges of the pore play in this process, it would be interesting to consider the same process with a polydisperse polymer brush, or with a predefined pattern of brushes of different height. These could be obtained, for instance by mixing two immiscible polymers of different height to promote their phase separation. It is important to stress that our system differs from the GroEL/GroES Chaperonin not only in the origin of the forces driving the possible translocation mechanism (fluid flow vs entropic confinement) but also in the nature of the brush. In fact, it is known that the biopolymers in the equatorial region of the GroEL/GroES complex have hydrophobic ends, which makes it much more likely for misfolded proteins to translocate compared to a correctly folded one. Both simulations and experiments of our system with weakly hydrophobic ends should be feasible and could provide a critical improvement to the purification process.

We would like to thank Peter van Oostrum, Erik Reimhult and Christoph Dellago for fruitful discussions and a critical reading of the manuscript. All simulations presented in this paper were carried out on the Vienna Scientific Cluster (VSC). We acknowledge support from the Austrian Science Fund (FWF) project 26253-N27. AC Acknowledges support from the National Science Foundation under Grant No. DMR-1703873

---

* Electronic address: icoluzza@cicbiomagune.es; Electronic address: ac2822@columbia.edu

[1] C. M. Dobson, A. Sali, M. Karplus, A. Šali, and M. Karplus, Angewandte Chemie - International Edition **37**, 868 (1998), ISSN 14337851, URL http://dx.doi.org/10.1002/(SICI)1521-3773(19980420)37:7%3C868::AID-ANIE868%3E3.0.CO2-H(null).

[2] M. Vendruscolo, E. Paci, C. M. Dobson, and M. Karplus, Nature **409**, 641 (2001), ISSN 00280836, URL http://www.ncbi.nlm.nih.gov/pubmed/11214326.

[3] M. Vendruscolo and C. M. Dobson, Faraday Discussions **143**, 277 (2009), ISSN 1359-6640, URL papers2://publication/doi/10.1039/b905825g.

[4] G. G. Tartaglia, S. Pechmann, C. M. Dobson, and M. Vendruscolo, Trends in Biochemical Sciences **32**, 204 (2007), ISSN 09680004, URL http://linkinghub.elsevier.com/retrieve/pii/S0968000407000655http://linkinghub.elsevier.com/retrieve/pii/

S0968000407000618.

[5] A. De Simone, C. Kitchen, A. H. Kwan, M. Sunde, C. M. Dobson, D. Frenkel, A. D. Simone, C. Kitchen, A. H. Kwan, M. Sunde, et al., Proceedings of the National Academy of Sciences of the United States of America **109**, 6951 (2012), ISSN 1091-6490, URL http://www.pubmedcentral.nih.gov/articlerender.fcgi?artid=3344965&tool=pmcentrez&rendertype=abstract%5Cnhttp://www.ncbi.nlm.nih.gov/pubmed/22509003http://www.pnas.org/cgi/doi/10.1073/pnas.1118048109.

[6] S. Gräslund, P. Nordlund, J. Weigelt, J. Bray, O. Gileadi, S. Knapp, U. Oppermann, C. Arrowsmith, R. Hui, J. Ming, et al., Nature Methods **5**, 135 (2008), ISSN 1548-7091, URL http://www.nature.com/doifinder/10.1038/nmeth.f.202.

[7] R. C. F. Cheung, J. H. Wong, and T. B. Ng, Applied microbiology and biotechnology **96**, 1411 (2012), ISSN 0175-7598.

[8] J. Frydman, Annual review of biochemistry **70**, 603 (2001), ISSN 0066-4154, URL http://www.ncbi.nlm.nih.gov/pubmed/11395418.

[9] A. Baumketner, A. Jewett, and J. E. Shea, Journal of Molecular Biology **332**, 701 (2003), ISSN 00222836, URL papers2://publication/doi/10.1016/S0022-2836(03)00929-Xhttp://linkinghub.elsevier.com/retrieve/pii/S002228360300929X.

[10] A. R. Kinjo and S. Takada, Biophysical journal **85**, 3521 (2003), ISSN 00063495, URL http://dx.doi.org/10.1016/S0006-3495(03)74772-9.

[11] T. R. Jahn and S. E. Radford, Archives of Biochemistry and Biophysics **469**, 100 (2008), ISSN 00039861, URL http://dx.doi.org/10.1016/j.abb.2007.05.015.

[12] I. Coluzza, A. De Simone, F. Fraternali, and D. Frenkel, PLoS Computational Biology **4**, e1000006 (2008), ISSN 1553734X, URL http://dx.doi.org/10.1371/journal.pcbi.1000006http://www.pubmedcentral.nih.gov/articlerender.fcgi?artid=2265519&tool=pmcentrez&rendertype=abstracthttp://dx.plos.org/10.1371/journal.pcbi.1000006.

[13] I. Coluzza, S. M. Van Der Vies, and D. Frenkel, Biophysical Journal **90**, 3375 (2006), ISSN 0006-3495, URL papers2://publication/uuid/CE800413-3EA1-49B8-9417-248AFE30787C%5Cnhttp://www.pubmedcentral.nih.gov/articlerender.fcgi?artid=1440723&tool=pmcentrez&rendertype=abstractpapers2://publication/uuid/CE800413-3EA1-49B8-9417-248AFE30787Chttp://www.pubmedcentra.

[14] C. A. Siedlecki, B. J. Lestini, K. Kottke-Marchant, S. J. Eppell, D. L. Wilson, and R. E.

Marchant, Blood **88**, 2939 (1996), ISSN 00064971.

[15] S. W. Schneider, S. Nuschele, A. Wixforth, C. Gorzelanny, A. Alexander-Katz, R. R. Netz, and M. F. Schneider, Proceedings of the National Academy of Sciences **104**, 7899 (2007), ISSN 0027-8424, URL http://www.pnas.org/cgi/doi/10.1073/pnas.0608422104.

[16] C. E. Sing and A. Alexander-Katz, Biophysical Journal **98**, L35 (2010), ISSN 00063495, URL http://dx.doi.org/10.1016/j.bpj.2010.01.032http://linkinghub.elsevier.com/retrieve/pii/S0006349510001979.

[17] I. B. Bekard, P. Asimakis, J. Bertolini, and D. E. Dunstan, Biopolymers **95**, 733 (2011), ISSN 00063525.

[18] J. Jaspe and S. J. Hagen, Biophysical Journal **91**, 3415 (2006), ISSN 00063495, URL http://linkinghub.elsevier.com/retrieve/pii/S0006349506720537.

[19] M.-B. Luo, D. A. Tsehay, and L.-Z. Sun, The Journal of Chemical Physics **147**, 034901 (2017), ISSN 0021-9606, URL http://aip.scitation.org/doi/10.1063/1.4993217.

[20] S. Egorov, A. Milchev, L. Klushin, and K. Binder, Soft Matter **7**, 5669 (2011), ISSN 1744683X 17446848.

[21] M. A. I. Mahmood, W. Ali, A. Adnan, and S. M. Iqbal, The Journal of Physical Chemistry B **118**, 5799 (2014), ISSN 1520-6106.

[22] A. Alexander-Katz, M. F. Schneider, S. W. Schneider, A. Wixforth, and R. R. Netz, Physical Review Letters **97**, 1 (2006), ISSN 00319007.

[23] I. V. Neratova, T. Kreer, and J.-U. Sommer, Macromolecules **48**, 3756 (2015), ISSN 0024-9297.

[24] Z. Posel, M. Svoboda, C. M. Colina, and M. Lísal, Soft Matter **13**, 1634 (2017).

[25] J. D. Honeycutt and D. Thirumalai, Biopolymers **32**, 695 (1992), ISSN 10970282, URL http://www.ncbi.nlm.nih.gov/pubmed/1643270.

[26] A. Lamura, G. Gompper, T. Ihle, and D. M. Kroll, EPL (Europhysics Letters) **56**, 319 (2001), ISSN 0295-5075.

[27] S. Plimpton, Journal of Computational Physics **117**, 1 (1995), ISSN 0021-9991.

[28] S. Alexander, Journal de Physique **38**, 983 (1977), ISSN 0302-0738, URL http://www.edpsciences.org/10.1051/jphys:0197700380809830 0%5Cnhttp://jphys.journaldephysique.org/articles/jphys/pdf/1977/08/jphys_1977__38_8_983_0.pdf%5Cnhttp://www.edpsciences.org/10.1051/jphys:01977003808098300.

[29] D. I. Dimitrov, A. Milchev, and K. Binder, Journal of Chemical Physics **125**, 34905 (2006), ISSN 00219606, URL papers2://publication/doi/10.1063/1.2211615.

[30] A. L. Yarin, Journal of Non-Newtonian Fluid Mechanics **37**, 113 (1990), URL http://www.sciencedirect.com/science/article/pii/037702579090001R.

[31] K. Binder, The European physical journal. E, Soft matter **9**, 293 (2002), ISSN 12928941, URL http://dx.doi.org/10.1140/epje/i2002-10076-2http://www.ncbi.nlm.nih.gov/pubmed/15010923.

[32] Y. Rabin and S. Alexander, Europhysics Letters (EPL) **13**, 49 (1990), ISSN 0295-5075, URL http://stacks.iop.org/0295-5075/13/i=1/a=009?key=crossref.cb1b376612c74c771a591de5adb6ebd5.

[33] D. F. Parsons and D. R. M. Williams, Physical Review E **74**, 041804 (2006), ISSN 1539-3755, URL https://link.aps.org/doi/10.1103/PhysRevE.74.041804.

SUPPLEMENTARY MATERIAL

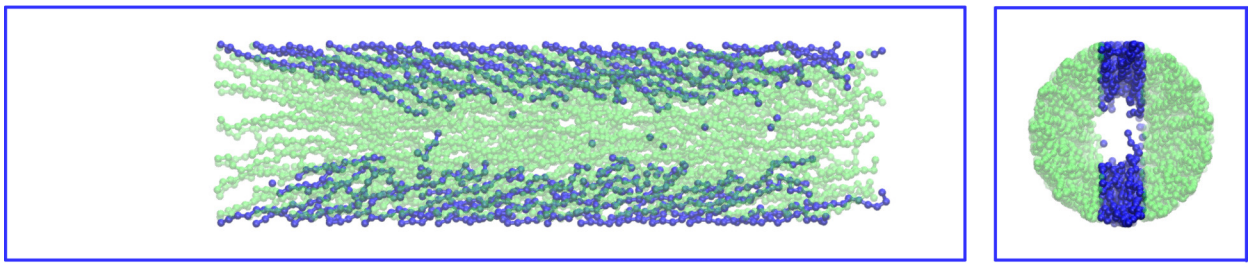

Supplemental Material, Figure S13: Snapshot of a cylindrical brush under flow for **Case 2** (see the methods section of the main text for pore parameters), showing the side view on the left panel and the cross section on the right panel. Several chains are depicted in blue to show individual chain conformations. Here, $N_m = 20$ and the flow acceleration $a = 0.1$ and $R = 9.55\sigma$.

APPENDIX

To quantify the overall behavior of the brush in the presence of the fluid flow, we measured the local brush tilt angle ϕ with respect to the cylinder axis along the direction of the flow $\vec{v} = (1, 0, 0)$. The direction of each polymer in the brush is defined by the vector connecting its grafting point and the last monomer. What follows is the quantitative analysis for the three pores considered in this study.

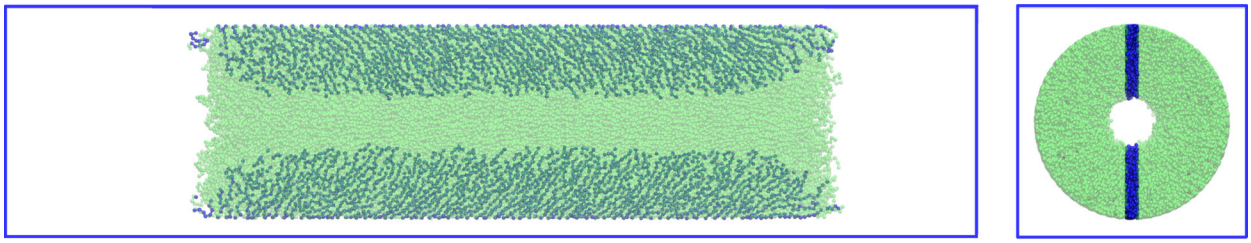

Supplemental Material, Figure S14: Snapshot of a cylindrical brush under flow for **Case 3** (see the methods section of the main text for pore parameters), showing the side view on the left panel and the cross section on the right panel. Several chains are depicted in blue to show individual chain conformations. Here, $N_m = 20$ and the flow acceleration $a = 0.1$ and $R = 19.1\sigma$.

Case 1

Figure S15 shows the brush alignment along the length of the pore for flows $a = 0, 0.01, 0.05, 0.1$ and for chain lengths $N_m = 10, 14$. Since we expect the middle of the

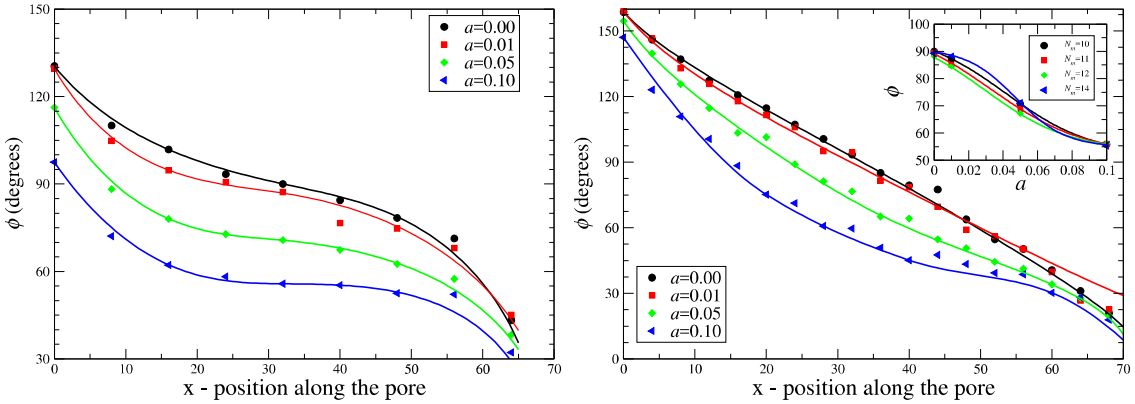

Supplemental Material, Figure S15: **Case-1**:Average tilt angle ϕ of the chains in the brush with respect to the direction of the flow for different flow accelerations a. The left panel shows the results for $N_m = 10$ and the right panel shows the results for $N_m = 14$. The inset shows how for different values of a, the brush tilt ϕ in the middle of the pore ($x = L_p/2$) is rather insensitive to the value of N_m. The lines are just guides for the eye.

brush ($x \simeq L_p/2$) to be less sensitive to the behavior of the pore edges, we also show in the inset of Fig. S15 how the tilt angle changes with the fluid acceleration in the middle of the brush for different values of N_m. Overall, we observe a systematic decrease of ϕ from the equilibrium value of 90 degrees with a. Finally, the inset shows how in the middle of the pore, ($x \simeq L_p/2$), ϕ seems to be rather insensitive to the chain length N_m.

Case 2

Figure S16 shows the brush alignment along the length of the pore for flows $a = 0, 0.01, 0.05, 0.1$ and for chain lengths $N_m = 30, 40$. Unlike the results for **Case 1**, at

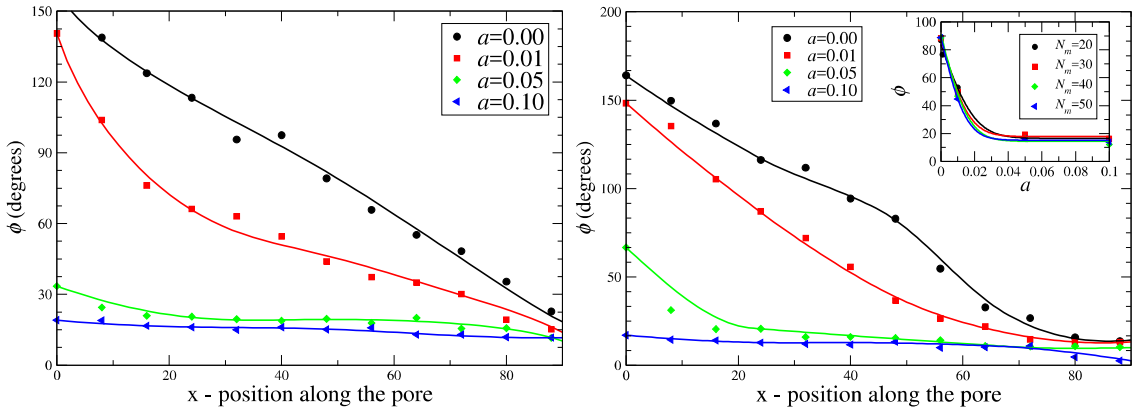

Supplemental Material, Figure S16: **Case-2**: Average tilt angle ϕ of the chains in the brush with respect to the direction of the flow for different flow accelerations a. The left panel corresponds to the case with $N_m = 30$, the other to the case with $N_m = 40$. The inset shows how ϕ changes with a for different values of N_m in the middle of the pore ($x = L_p/2$). The lines lines are just guides for the eye.

this low grafting densities, already for $a \geq 0.05$ the brush acquires a clear tilt angle that is roughly constant throughout the length of the pore. As in the previous case, we observe a systematic decrease of ϕ from the equilibrium value of 90 degrees with a until it saturates to a value of about 20 degrees. Finally, the inset shows how in the middle of the pore, ($x \simeq L_p/2$), ϕ seems to be rather insensitive to the chain length N_m.

Case 3

Figure S17 shows the brush alignment along the length of the pore for flows ranging from $a = 0$ to $a = 0.1$. and for chain lengths $N_m = 20, 24$. The front of the pore is characterized by a layer of polymers that resist pointing in the direction of the flow even at the highest driving forces (this effect becomes more evident as one increases N_m) while the back side of the brush can easily adapt to the direction of the flow. Overall, even in this case, we observe a systematic decrease of ϕ from the equilibrium value of 90 degrees with a. Finally, the inset shows how the tilt angle of the brush along the direction of the flow in the middle

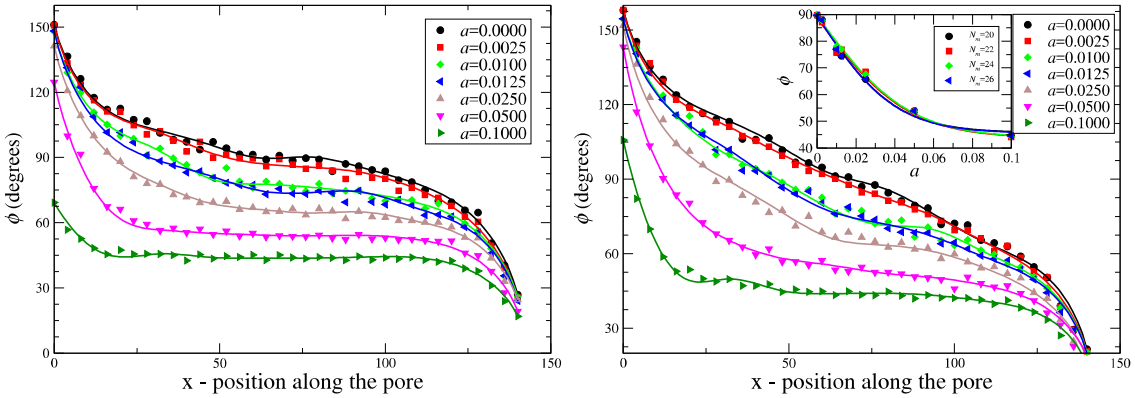

Supplemental Material, Figure S17: **Case-3**: Average tilt angle ϕ of the chains in the brush with respect to the direction of the flow for different flow accelerations a. The left panel corresponds to the case with $N_m = 20$, the other to the case with $N_m = 24$. The inset shows how ϕ changes with a for different values of N_m in the middle of the pore ($x = L_p/2$). The lines lines are just guides for the eye.

of the pore changes as a function of a, and again, we observe that ϕ is basically independent of the number of monomers in the polymer brush, N_m.